Functional brain networks and neuroanatomy underpinning nausea severity can predict nausea susceptibility using machine learning

James K. Ruffle[1] 🆔, Anya Patel[1], Vincent Giampietro[2], Matthew A. Howard[2], Gareth J. Sanger[1] 🆔, Paul L. R. Andrews[3], Steven C. R. Williams[2], Qasim Aziz[1] and Adam D. Farmer[1,4,5]

[1]*Centre for Neuroscience and Trauma, Blizard Institute, Wingate Institute of Neurogastroenterology, Barts and the London School of Medicine & Dentistry, Queen Mary University of London, 26 Ashfield Street, London E1 2AJ, UK*

[2]*Department of Neuroimaging, King's College London, Institute of Psychiatry, Psychology & Neuroscience, London SE5 8AF, UK*

[3]*Division of Biomedical Sciences, St George's University of London, London SW17 0RE, UK*

[4]*Institute of Applied Clinical Sciences, University of Keele, Keele ST5 5BG, UK*

[5]*Department of Gastroenterology, University Hospitals of North Midlands NHS Trust, Stoke on Trent ST6 8QG, UK*

Edited by: Kim Barrett & David Grundy

The Journal of Physiology

Key points

- Nausea is an adverse experience characterised by alterations in autonomic and cerebral function.
- Susceptibility to nausea is difficult to predict, but machine learning has yet to be applied to this field of study.
- The severity of nausea that individuals experience is related to the underlying morphology (shape) of the subcortex, namely of the amygdala, caudate and putamen; a functional brain network related to nausea severity was identified, which included the thalamus, cingulate cortices (anterior, mid- and posterior), caudate nucleus and nucleus accumbens.
- Sympathetic nervous system function and sympathovagal balance, by heart rate variability, was closely related to both this nausea-associated anatomical variation and the functional connectivity network, and machine learning accurately predicted susceptibility or resistance to nausea.
- These novel anatomical and functional brain biomarkers for nausea severity may permit objective identification of individuals susceptible to nausea, using artificial intelligence/machine learning; brain data may be useful to identify individuals more susceptible to nausea.

Abstract Nausea is a highly individual and variable experience. The central processing of nausea remains poorly understood, although numerous influential factors have been proposed, including

James K. Ruffle is an Academic Clinical Fellow in clinical radiology at University College London Hospitals NHS Trust and honorary research fellow in neurogastroenterology at the Wingate Institute of Neuro-gastroenterology, Blizard Institute, Queen Mary University of London. His work involves the neurobiology of visceral sensations, including nausea and pain, and includes use of neuroimaging and data-science-driven techniques. **Anya Patel** is medical student at the University of Birmingham. She undertook analysis of this data for her Neuroscience BSc project thesis at Barts and the London School of Medicine and Dentistry, Queen Mary University of London.

J. K. Ruffle and A. Patel are joint first authors. Q. Aziz and A. D. Farmer are joint senior authors.

brain structure and function, as well as autonomic nervous system (ANS) activity. We investigated the role of these factors in nausea severity and if susceptibility to nausea could be predicted using machine learning. Twenty-eight healthy participants (15 males; mean age 24 years) underwent quantification of resting sympathetic and parasympathetic nervous system activity by heart rate variability. All were exposed to a 10-min motion-sickness video during fMRI. Neuroanatomical shape differences of the subcortex and functional brain networks associated with the severity of nausea were investigated. A machine learning neural network was trained to predict nausea susceptibility, or resistance, using resting ANS data and detected brain features. Increasing nausea scores positively correlated with shape variation of the left amygdala, right caudate and bilateral putamen (corrected $P = 0.05$). A functional brain network linked to increasing nausea severity was identified implicating the thalamus, anterior, middle and posterior cingulate cortices, caudate nucleus and nucleus accumbens (corrected $P = 0.043$). Both neuroanatomical differences and the functional nausea-brain network were closely related to sympathetic nervous system activity. Using these data, a machine learning model predicted susceptibility to nausea with an overall accuracy of 82.1%. Nausea severity relates to underlying subcortical morphology and a functional brain network; both measures are potential biomarkers in trials of anti-nausea therapies. The use of machine learning should be further investigated as an objective means to develop models predicting nausea susceptibility.

Introduction

Nausea is an unpleasant experience that can precede vomiting and is amongst the most common and distressing gastrointestinal (GI) symptoms. The causes of nausea are diverse and include intrinsic gastroenterological disorders (e.g. gastroparesis), motion sickness and pregnancy, and it is a frequent side-effect of medications including chemotherapeutic and anaesthetic agents (Stern *et al.* 2011). Nausea has a population prevalence of 14% reported in a community based survey (Haug *et al.* 2002). Although nausea is a common clinical symptom, anti-emetics have limited efficacy against nausea and treatments targeted specifically against nausea, irrespective of cause, are lacking (Sanger & Andrews, 2018).

There is marked intra- and inter-individual variability in both susceptibility to nausea and the severity that individuals experience. Indeed, a number of factors have been proposed to influence an individual's experience of nausea, including demographics, autonomic nervous system (ANS) activity, and brain processing (Stern *et al.* 2011). Converging evidence suggests that the experience of nausea involves bidirectional interactions within the brain-gut axis involving the central nervous system (CNS), autonomic nervous system, gastrointestinal physiology (including gastric dysrhythmia) and endocrine pathways (Muth, 2006; Napadow *et al.* 2013*a,b*; Andrews & Sanger, 2014; Angeli *et al.* 2015; Farmer *et al.* 2015).

The lack of understanding of the central mechanisms of nausea is partially a consequence of the inherent challenges of studying it, given that animal models are significantly limited in their translational potential of a subjective and interoceptive human experience (Andrews & Sanger, 2014; Aziz & Ruffle, 2018). In human experimentation, nausea can be physiologically induced as a consequence of motion sickness, either by actual motion (Coriolis–cross-coupled stimulus (Miller & Graybiel, 1970)) or through illusory self-motion, an epiphenomenon referred to as 'vection' (Koch, 1999). Nausea stimulated by vection is a form of visually induced motion sickness (VIMS), similar to true motion sickness insofar as it induces nausea and, at its most intense level, vomiting (Muth, 2006; Shupak & Gordon, 2006; Kennedy *et al.* 2010).

Current understanding of the CNS changes that accompany the development and severity of nausea that individuals experience remains limited. Although functional neuroimaging techniques have been applied to the study of nausea (Napadow *et al.* 2013*b*; Farmer *et al.* 2015; Toschi *et al.* 2017), they remain relatively scarce in comparison to those evaluating other aspects of GI sensation, such as visceral pain (Ruffle *et al.* 2017). In previous studies utilising functional magnetic resonance imaging (fMRI), researchers variably demonstrated nausea-related activation of a number of brain areas salient to interoception such as the amygdala, putamen, pons, locus coeruleus, and others associated with fear conditioning, such as the anterior insula and middle cingulate (Napadow *et al.* 2013*b*; Farmer *et al.* 2015; Sclocco *et al.* 2016; Toschi *et al.* 2017). Furthermore, neuroanatomical differences in white matter tracts have also been associated with increased nausea

susceptibility (Napadow *et al.* 2013*a*). However, whilst certainly providing some insight into CNS mechanisms, existing studies are limited and have largely focused on the identification of singular brain regions involved in nausea (Farmer *et al.* 2015), or pairwise connectivity between two areas (Toschi *et al.* 2017). Given the complexity of the sensation of nausea, it seems likely that the physiological and interoceptive components of a nauseous experience are a result of many brain areas interacting in synchrony. To date, there remains minimal understanding of such networks associated with nausea. In addition, it is unknown whether patient stratification into those with and without nausea susceptibility can be achieved using machine learning based on these aforementioned brain differences.

Thus, the aims of the present study were threefold. Firstly, given that some individuals are significantly more susceptible to nausea than others, we hypothesised that this could be attributed to differences in the brain structure engendering the central autonomic network (Critchley & Harrison, 2013). We therefore investigated subcortical brain morphological differences in individuals of varying sensitivities to nausea induced by visually-induced motion sickness. Secondly, we hypothesised that the complex experience of nausea is processed by multiple brain regions interacting synchronously as a functional network, which we aimed to probe with network-based statistics. Thirdly, as a proof of concept, we investigated whether patient stratification into those susceptible and resistant to nausea can be accurately predicted by artificial intelligence/machine learning (see Russell & Norvig, 2009; Dey, 2016; Ruffle *et al.* 2018*d*), using brain (neuroanatomical and functional connectomic) and ANS data alone.

Methods

Ethical approval

All protocols were approved by King's College London Research Ethics Committee (ref: PNM/09/09-04). Written informed consent was obtained from all participants, and all studies conformed to the standards set by the latest revision of the *Declaration of Helsinki*. All participants were naïve to the experimental protocols.

Study population

Twenty-eight healthy participants (15 male), aged 18–65 years (mean age 24 years), who had no known past medical history and were not currently taking any prescribed or over-the-counter medications, took part in the study. All were non-smokers and were asked to avoid caffeine and alcohol for 24 h prior to the study. Females of child bearing potential were studied in the follicular stage of their menstrual cycle. The validated Hospital Anxiety and Depression Scale was used to screen for sub-clinical anxiety and depression (Zigmond & Snaith, 1983). All participants were right handed, as screened by the Edinburgh Handedness Inventory (Oldfield, 1971). Participants were studied in the afternoon (between 14.00 and 16.00 h) in a temperature-controlled thermoneutral (20–22°C) environment. Aspects of the experimental data have been published previously by our group (Farmer *et al.* 2015), though for entirely disparate analytical investigations which are not reported in this manuscript.

Induction of nausea

We utilised a previously validated visual stimulus (Farmer *et al.* 2015), a 10-min video of a landscape (London Eye, Houses of Parliament) as seen from a point 2 m above the centre of Westminster Bridge, London, UK. The video was composed with a sequence of digital camera images taken from the viewpoint of a tall subject standing on the bridge. The point of view rotated, panning the scene through 360 deg at a rate of 0.2 Hz about an axis tilted 18 deg from earth vertical. The tilted and rotated visual display instigates the perception of spinning on the spot about a tilted axis due to vection. Viewing a moving tilted scene has been shown to enhance the onset of visually induced motion sickness (Bubka & Bonato, 2003). A similar stimulus has previously been used to induce visually induced motion sickness (Golding *et al.* 2012), and in our own laboratory produced an effective nauseogenic stimulus with this same paradigm (Farmer *et al.* 2015). For fMRI, participants wore a pair of MR-compatible goggles (CinemaVision, Salvadorini Consulting LLC, Lexington, NC, USA) and were positioned supine in the MRI scanner. The goggles were used to project the motion video to the participant during scanning, allowing an unimpeded view of the stimulus. During the active scanning phase, the 10 min motion video was projected through the goggles. Throughout the study, participants were instructed to remain still and to focus on the stimulus. On a separate day of scanning, participants underwent a second MRI wherein they viewed a static single image of this 10 min video, which was used as a control for statistical comparison. Whether a participant would view the control or the motion video first was pseudorandomised.

During the motion video, experience of nausea was assessed using a 4-point visual analogue scale (VAS), where 1 represented no symptoms and a score of 4 represented severe nausea. The validated motion sickness sensitivity score (MSSQ) (Golding, 1998) and motion sickness assessment questionnaire (MSAQ) (Gianaros *et al.* 2001) were used to assess susceptibility to and symptoms associated with motion sickness, respectively. The MSSQ questionnaire asks participants to rate their previous experiences of nausea as a child, and over the last

10 years, across 9 different situations, such as in a car, on a bus, on a train etc, scored on a 5-point Likert scale ranging from not applicable to frequently felt sick (Golding, 1998). The MSAQ evaluates the experience of motion sickness across GI, central, peripheral and sopite-related dimensions by asking participants to rate their sickness using a 9-point scale across 16 items (Gianaros *et al.* 2001).

Assessment of autonomic activity by heart rate variability

Resting autonomic parameters were derived from heart rate variability (HRV) measures, in accordance with international recommendations (European Society of Cardiology, 1996). In a quiet thermoneutral laboratory environment (to prevent MR scanner-related confounds), ECG electrodes (Ambu Blue Sensor P, Denmark) were placed at the cardiac apex, left and right sub-clavicular areas of each participant for ECG signal acquisition. ECG readings were digitally recorded using a bio-signals acquisition system (Neuroscope, Medifit Instruments, Enfield, Essex, UK) at 5 kHz. Resting autonomic activity was derived by validated non-invasive HRV cardio-metrics; parasympathetic nervous system (PNS) activity by putative measure of efferent brainstem cardiac vagal tone (CVT) and sympathetic nervous system (SNS) activity by cardiac sympathetic index (CSI) (Julu, 1992; Toichi *et al.* 1997). Sympathovagal balance was also approximated by the ratio between CSI (sympathetic) and CVT (parasympathetic). After attachment of all autonomic recording apparatus, data were recorded for 5 min with participants asked to relax (but not fall asleep), during which *resting* autonomic tone was derived. We have previously used this same method of quantifying resting autonomic measures for application to MRI data (see Ruffle *et al.* 2018*b,c*).

Parasympathetic nervous system: derivation of resting cardiac vagal tone. The derivation of resting parasympathetic activity by CVT is described in detail elsewhere (Farmer *et al.* 2014). In brief, the incoming QRS complex is compared to a unique template, generated from the initial acquisition of the ECG from the individual. If the QRS complexes are sufficiently comparable, voltage gated oscillators within the Neuroscope generate a 1 mV pulse, which feeds to a two-limb circuit, consisting of a high-pass and low-pass limb. The high-pass limb precisely follows the incoming QRS signal, whilst the low-pass limb produces a damped rendition (Little *et al.* 1999). Therefore, the lesser the delta change of an incoming signal, that is to say the lower the HRV, the more closely the low-pass limb will mimic the high-pass limb, resulting in a lower value. In contrast, the greater the HRV the more the low-pass limb will deviate from its

high-pass counterpart, resulting in a higher value. This phenomenon is referred to as 'phase shift demodulation' and is uniquely based upon non-invasive measures of PNS tone. CVT is measured on a linear vagal scale (LVS), where a value of 0 is derived from fully atropinised healthy human volunteers (Julu & Hondo, 1992; Farmer *et al.* 2014). Moreover, mathematically CVT correlates closely to other putative 'parasympathetic' measures, including both HRV and root mean square of successive differences (RMSSD) (Brock *et al.* 2017).

Sympathetic nervous system: cardiac sympathetic index. Resting sympathetic nervous system (SNS) activity was quantified by means of the cardiac sympathetic index (CSI). To determine CSI, R-R interval data were first extracted from the ECG and manually reviewed to remove any artefacts. Subsequently, R-R data were transferred to the cardiac metric program, which yields a calculation of the validated Toichi's cardiac sympathetic index by use of the Lorenz plot (Toichi *et al.* 1997). Notably, CSI is disparate to low frequency (LF) band analysis of HRV, and demonstrated as superior to LF in ascertaining sympathetic function by Toichi *et al.* (1997). CSI is the ratio of R-R intervals and thus has no units (Farmer *et al.* 2013).

MRI acquisition

MRI data were collected on a General Electric Signa Excite II 1.5 Tesla HD scanner located at the Centre for Neuro-imaging Sciences, Institute of Psychiatry, Psychology & Neuroscience, King's College London. Head movement was minimised by application of foam padding within the head coil and an eye movement tracker was mounted onto the head coil. For each participant, structural brain data were acquired via a high resolution T1-weighted 3D FSPGR structural scan, in sagittal orientation, using the following parameters: repetition time (TR) 7.02 ms; echo time (TE) 2.82 ms; inversion time (TI) 450 ms; slice thickness 1.1 mm; field of view 280 mm; flip angle 208; spatial positions 196; image matrix $256 \times 256 \times 196$ voxels; in plane voxel dimensions $1.1 \times 1.1 \times 1.1$ mm. During fMRI, 300 T2*-weighted images per slice (40×3 mm slices, 0.3 interslice gap, TE 25 ms, TR 3500 ms, flip angle 90 deg, matrix 64^2), depicting blood oxygen level dependent (BOLD) contrast, were collected as participants viewed the motion video.

Pre-processing of structural MRI data

Raw structural MRI images were first carefully manually reviewed to check for signal and image artefacts that may otherwise confound findings. Subsequently, subcortical structural pre-processing (for analysis of

morphology/shape) was conducted using FSL-FIRST 5.0, an algorithm that uses Bayesian statistics for automated brain segmentation (Patenaude *et al.* 2011). This approach identifies and segments each anatomical scan into 15 subcortical regions: bilateral nucleus accumbens, amygdala, caudate, hippocampus, pallidum, putamen and thalamus, plus the brainstem. All scans were registered to 1 mm standard space (Montreal Neurological Institute (MNI) 152), to account for overall differences in the shape and size of each subject's skull and brain. Both registrations (whole scan and ROI) were manually checked for correct template-scan alignment. Individual resultant subcortical nuclei were concatenated to a single 4D structural file (1 volume per subject) to permit statistical analysis. Additionally, volumetric data (in mm^3) were also extracted from these regions for *post hoc* machine learning feature synthesis (see later). All statistical analysis of structural MR data was undertaken with general linear modelling (GLM) against nausea VAS scores, wherein demeaned demographical covariates, age and gender, were included as nuisance regressors.

Pre-processing of functional MRI data

fMRI data pre-processing was undertaken using FMRI Expert Analysis Tool (FEAT) version 5.98, part of the FMRIB Software Library (FSL) software package (www.fmrib.ox.ac.uk/fsl) (Smith *et al.* 2004). The following pre-statistics processing was applied: Motion Correction with FMRIB Linear Image Registration Tool (MCFLIRT) (7 degrees of freedom); slice-timing correction using Fourier-space time-series phase-shifting; brain extraction (BET); spatial smoothing using a Gaussian kernel of full-width-half-maximum (FWHM) 5 mm; grand-mean intensity normalisation of the entire 4-dimensional dataset by a single multiplicative factor; high pass temporal filtering (Gaussian-weighted least-squares straight line fitting, with sigma = 50.0s). Registration to high resolution structural and standard space images was carried out using the FMRIB Linear Image Registration Tool (FLIRT).

Network-based statistics

Using *a priori* selection of regions (Stern *et al.* 2011; Critchley & Harrison, 2013), 22 regions of interest (ROI) parcellation masks were generated using the Harvard-Oxford Cortical Structural Probability Atlas and FSLeyes (Smith *et al.* 2004), to identify regions for extraction of functional activity data. Masks were thresholded to a maximal region probability of $\geq$65%, binarised, and aligned to their specific anatomical areas on each individual's scan. The 22 functional ROIs included 14 of the aforementioned structurally segmented subcortical ROIs: bilateral nucleus accumbens, amygdala,

caudate, hippocampus, pallidum, putamen and thalamus. Furthermore, the hypothalamus, bilateral insula, bilateral orbitofrontal cortex and anterior (ACC), middle (MCC) and posterior cingulate cortices (PCC) were added. Within FSLeyes, the Talairach brain map was used to delineate the hypothalamus, as presently no Harvard map exists for this region (Talairach & Tournoux, 1988); this approach is in keeping with previous fMRI studies investigating this brain structure (Baroncini *et al.* 2012). Brainstem sub-regions were *omitted* from the network-based analysis as we felt it was questionable whether the resolution of the scanner would permit stringent analysis of such small brainstem nuclei (such as the nucleus tractus solitarius). The inclusion of ROIs in investigating for a role in the brain processing of nausea was also cross-referenced with NeuroSynth to provide insight to any possible confounds of the data (such as additional roles of the brain regions, for example in visual processing) (Yarkoni *et al.* 2011). Using MATLAB (version 2018a, https://uk.mathworks.com), the BOLD signal from each ROI, or 'node', was cross-correlated, producing correlation matrices of 55 node-node connective correlation (r) values, or 'edges' (resultant of binomial coefficient $\binom{22}{2} = 231$; or 22 "*choose*" 2). Our specific aim was to investigate functional connectivity between these areas and thus we did not statistically test activity of singular regions (such as the ACC). The rationale for this is because previous findings of brain activity to nauseogenic stimuli are already reported elsewhere, including with this experimental paradigm (Farmer *et al.* 2015).

The Network Based Statistics (NBS) connectome toolbox (version 1.2, https://www.nitrc.org/projects/nbs/) was used to investigate brain network differences contingent on the severity of nausea experienced during the motion video (Zalesky *et al.* 2010). The NBS is a non-parametric statistical method which corrects for multiple comparisons, and controls for the family-wise error rate (FWER). The NBS is the graph analogue of cluster-based statistical methods used in mass univariate testing on all voxels in an image and produces clusters in topological space (as opposed to physical space). NBS relies on permutation testing (Freedman & Lane method: Freedman & Lane, 1983) to determine significance within GLM, which includes regression of nuisance predictors, permuting resulting residuals and subsequently adding permuted residuals back to nuisance signal to give a realisation of data under the null hypothesis. This approach recognizes that permuting raw data is not desirable as it may engender some variability explained by nuisance predictors. It is rather the error terms that can be permuted and estimated under the null hypothesis as a part of the data not explained by the nuisance regressors; that is, the residuals (Anderson & Robinson, 2008). The method permits derivation of FWER-corrected *P* values using permutation testing when investigating

brain networks with fMRI (Sporns *et al.* 2005). The performed NBS analyses were linear contrasts of nausea VAS scores by GLM (with demeaned demographical nuisance covariates added), using 10,000 permutations and the criteria for significance set to FWER-corrected *P* < 0.05. Motion video analyses were also statistically compared to the control period to limit for an attention- or gaze-driven confound. A primary edge parameter threshold of 2.64 was used to accommodate for a Cohen's *d* medium-effect size of 0.5 (Zalesky *et al.* 2010). Results were visualized using the BrainNet illustrative package (http://www.nitrc.org/projects/bnv/) (Xia *et al.* 2013).

Analysis of demographic and psychophysiological data

Normality distributions of autonomic, demographic and psychophysiological data were tested using the Shapiro-Wilk normality test. *P* < 0.05 was adopted as the criterion to indicate statistical significance. Parametric statistical analyses of autonomic, nausea VAS and relationship to neuroimaging data found (including network properties) were performed using MATLAB (version 2018a, https://uk.mathworks.com), IBM SPSS Statistics (IBM Corp. Released 2017, Version 25.0. Armonk, NY: IBM Corp) and GraphPad Prism (version 6.00, GraphPad Software, La Jolla California, USA, www.graphpad.com).

Machine learning – neural network development

A machine learning approach was used as a *post hoc* proof of concept (Ruffle *et al.* 2018*d*). Our principal aim was to establish if susceptibility or resistance to nausea (by virtue of VIMS) could be accurately predicted from neuro-quantitative data. This was undertaken using the MATLAB statistics and machine learning toolbox, with a shallow neural network and scaled conjugate gradient backpropagation learning. Predictive features for the model were neuroanatomical, connectivity and autonomic (both parasympathetic and sympathetic) in nature, determined from aforementioned analyses undertaken. Additional feature synthesis was undertaken by determining subcortical volumetric symmetry ratios. The response target to be predicted by the model was susceptibility or resistance to nausea, which was binarised so that a minimum VAS score of 1 was equivalent to nausea-resistance (0) and VAS scores > 1 indicated nausea-susceptibility (+1). Five neurons were allocated to the hidden layer of the machine learning's neural network. Model hidden layer processing included sigmoid positive transfer function and sigmoid symmetric transfer function steps. Data were partitioned randomly to 70% for model training, 15% for model validation and the final 15% for model testing, as per conventional standard (Russell & Norvig, 2009; Dey, 2016). Model validation was undertaken with cross-entropy as per default toolbox settings.

Results

MSSQ score is a poor predictor of nausea severity

MSSQ (susceptibility to motion sickness by recollection of previous experiences) was not significantly correlated with either VAS or MSAQ (MSSQ and VAS: $r = 0.34$, $P = 0.08$; MSSQ and MSAQ: $r = 0.25$, $P = 0.20$) (Supporting information, Supplementary Fig. S1), indicative that the MSSQ is a poor predictive scoring system for determining nausea severity; at least in this sample and in response to this stimulus.

Resting sympathetic nervous system activity, assessed by the cardiac sympathetic index, relates to reported severity of nausea

Severity of nausea reported (VAS) during fMRI was significantly positively correlated to resting CSI (sympathetic tone) ($r = 0.43$, $P = 0.023$) (Fig. 1*A*). Resting CVT (parasympathetic) did not significantly correlate to the nausea VAS ($r = -0.32$ $P = 0.095$) (Fig. 1*B*). CSI/CVT ratio (sympathovagal balance) at rest was significantly positively correlated to severity of nausea experienced ($r = 0.42$, $P = 0.026$) (Fig. 1*C*).

Subcortical shape, but not volume, differs according to the severity of nausea experienced

Vertex (shape) analysis showed that morphological differences of the left amygdala, right caudate and bilateral putamen were significantly related to increasing nausea severity (threshold free cluster enhancement (TFCE)-corrected $P = 0.05$) (Fig. 2; Supporting information, Supplementary Video S1). There were no significant variations in morphology (shape) associated with *decreasing* nausea severity. There were no significant correlations between raw subcortical structure volumes and nausea VAS.

Nausea-related shape of the subcortex is sympathetically related by the cardiac sympathetic index

In *post hoc* analyses, we sought to investigate if these nausea-related morphological changes could be partially related to the HRV measures of autonomic nervous system (Ruffle *et al.* 2018*b*). In particular, we repeated GLM with alternate regression control for CVT

(parasympathetic) and CSI (sympathetic). Interestingly, these aforementioned morphological changes of the sub-cortex remained significant, despite nuisance covariate regression for CVT. However, with regression for CSI, the shape changes of the left amygdala, putamen and right caudate became non-significant, while the right putamen remained significant. This suggests that these nausea-related neuroanatomical differences could closely align to CSI (sympathetic) function.

A functional brain network relates to nausea severity

A significant functional brain network was identified that positively correlated with nausea severity (FWER-corrected $P = 0.043$) (Fig. 3). When thresholded to a Cohen's d of 0.5 (medium effect size), this network comprised 7 nodes with 7 functional connections ('edges') (Fig. 3A; Supporting information, Supplementary Video S1). Brain regions implicated were: ACC, MCC, PCC, left and right thalamus; right caudate and right nucleus accumbens. Significant edges (functional connections) of this network were the following: PCC-MCC; left thalamus-MCC; right thalamus-MCC; left thalamus-ACC; MCC-right caudate; MCC-nucleus accumbens and ACC-right caudate. Edge strengths defined as the degree of relationship in nausea severity to functional connectivity are listed in Fig. 3B and C. In comparison, there was no significant functional network identified when viewing the control video ($P = 1.00$).

Brain networks of nausea severity relate to resting autonomic measures of heart rate variability

Relationships between nausea network connectivity CSI (sympathetic), CVT (parasympathetic) and CSI/CVT ratio (sympathovagal balance) were investigated further. We found a highly significant (albeit weak) positive correlation between total network connectivity and resting CSI ($r = 0.24$, $P = 0.0008$) as well as the CSI/CVT ratio ($r = 0.21$, $P = 0.003$). A correlation between network connectivity and resting CVT was not apparent ($r = -0.13$, $P = 0.07$). In exploratory *post hoc* analyses, a machine learning stepwise linear model built a weak, albeit significant, linear model of resting CSI, using this nausea-related network connectivity data ($F_{4,60}$, $P = 0.04$). Furthermore, individual functional connections of the brain network and their relation to autonomic measures of
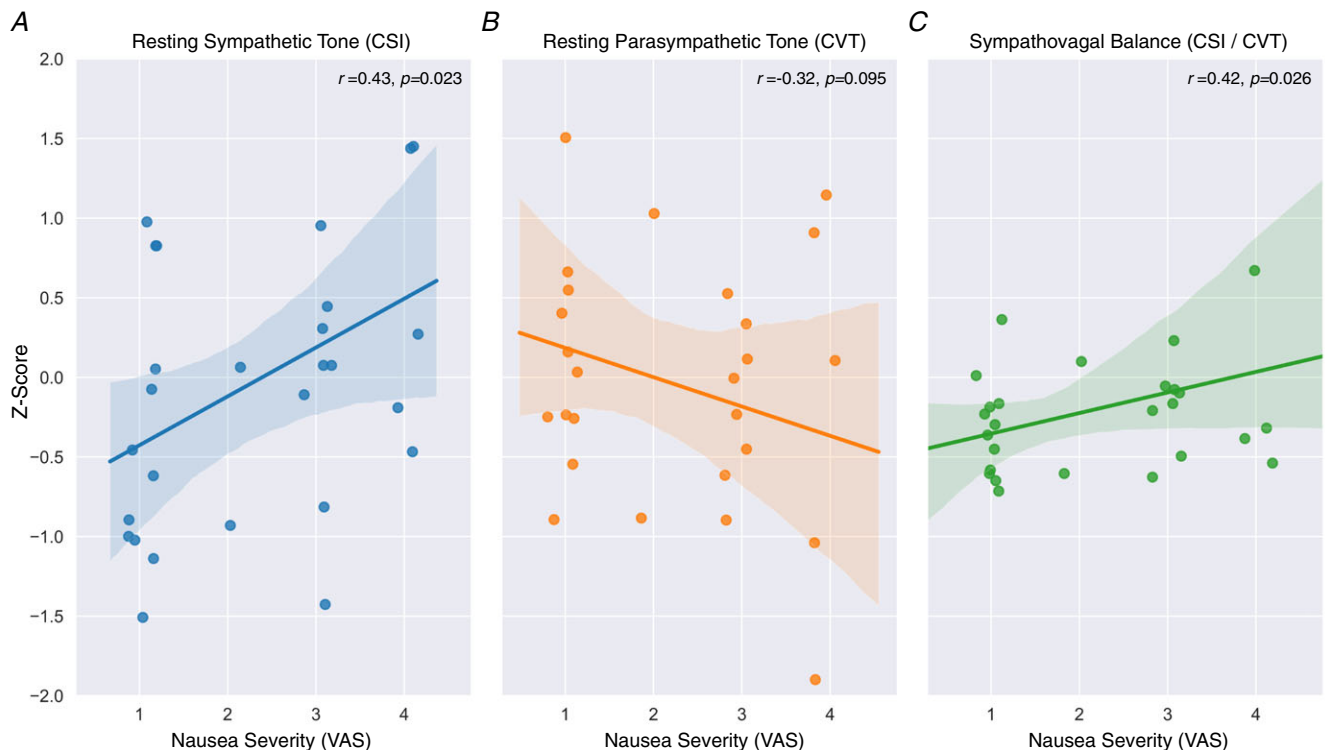

Figure 1. Severity of nausea and relationship to resting autonomic nervous system function
Both resting sympathetic tone (*A*) and sympathovagal balance (*C*) are significantly positively correlated to nausea severity during scanning, whilst a non-significant negative correlative trend for resting parasympathetic tone was apparent (*B*). Data *Z*-scored for illustrative purposes. $n = 28$. Line of best fit from linear regression with python robust outlier fitting, shaded area represents 95% confidence interval. Abbreviations: CSI, cardiac sympathetic index; CVT, cardiac vagal tone; VAS, visual analogue scale. [Colour figure can be viewed at wileyonlinelibrary.com]

HRV are available in the Supporting information section (Supplementary Figs S2–S4).

Machine learning predicts susceptibility to nausea from brain and autonomic data: a proof of concept

A predictive model for binary susceptibly to nausea (i.e. susceptible *vs.* resistant) was developed by virtue of a shallow neural network (Ruffle *et al.* 2018*d*). Predictive inputs to the neural network comprised aforementioned functional connectivity, neuroanatomical data and resting HRV measures of the ANS (Fig. 4*A*). The model was trained on 70% of the data (partitioned by random data division), which trained to an accuracy of 80% (area under curve (AUC) 0.80) (Fig. 4*B*). When testing the model with the remaining unseen data, it accurately allocated an individual to the nausea-resistant or susceptible category with an accuracy of 100% (AUC 1.00) (Fig. 4*C*). The total accuracy for all data, irrespective of data partition, was 82.1% (AUC 0.82) (Fig. 4*D*–*E*). Total true positive (TPR) and false negative rate (FNR) for nausea susceptibility was 100% and 0%, respectively. TPR and FNR for nausea resistance were 58.3% and 41.7%, respectively. Total positive predictive value (PPV) for nausea susceptibility was 76.2% (false discovery rate (FDR) for nausea resistance = 23.8%), whilst negative pre-dictive value (NPV) for nausea resistance was 100% (FDR for nausea susceptibility = 0%).

Discussion

Nausea is a complex and troublesome symptom and the central brain mechanisms responsible remain incompletely characterised. This study builds upon contemporaneous research and adds the following novel findings: (i) identification of a relationship between underlying subcortical neuroanatomy and nausea severity, (ii) delineation of a novel functional brain network relating to the severity of nausea experienced, (iii) interrelationships between nausea severity, autonomic neurophysiology, brain structure and connectivity, and (iv) identifying how coalescence of these findings can be used to predict susceptibility to nausea by artificial intelligence/ machine learning, as a proof of concept. We elaborate on these four key findings below.

A neuroanatomical predisposition to nausea

An individual's cross-sensitivity to differing nausea stimuli exhibits similarity, meaning that if an individual was sensitive to a given nauseogenic stimulus, such as motion sickness, they are typically sensitive to other nauseogenic
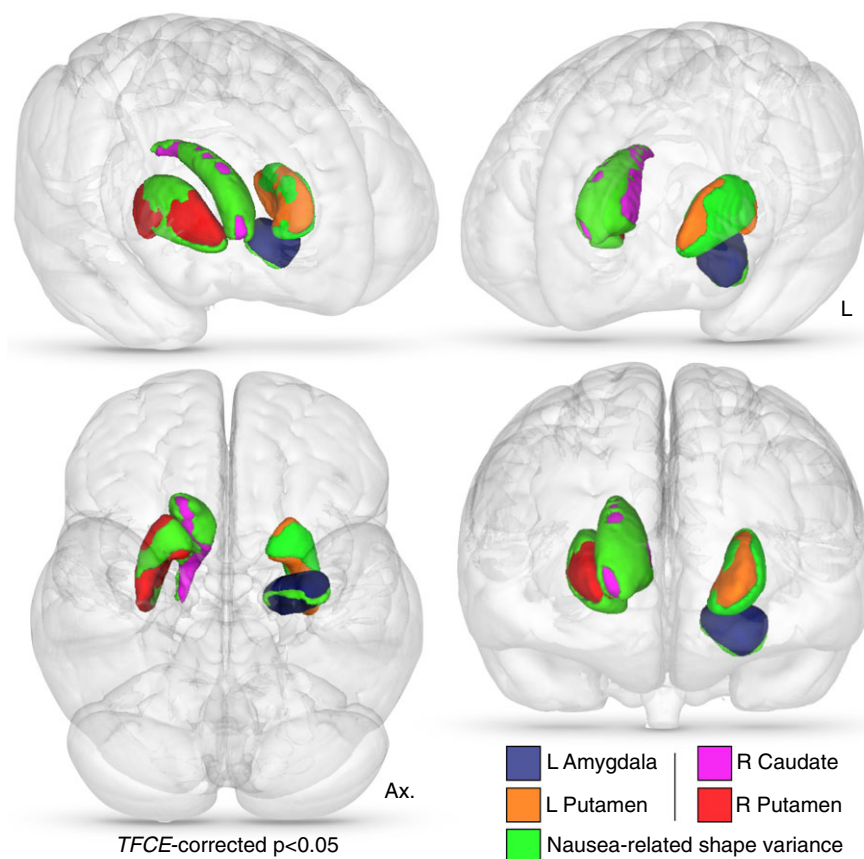

Figure 2. Nausea-related subcortical shape variance
Vertex deformation (shape) variance which positively related to increasing nausea severity. Subcortical masks colour-coded as per the given key, with overlaid aspects of nausea-related morphology. Statistical significance is TFCE-corrected and further thresholded to display only vertices of corrected *P* < 0.05. Abbreviations: Ax, axial. L, left; R, right; TFCE, threshold free cluster enhancement. [Colour figure can be viewed at wileyonlinelibrary.com]

L Amygdala | R Caudate
L Putamen | R Putamen
Nausea-related shape variance

TFCE-corrected p<0.05

stimuli, such as chemotherapy-induced nausea and vomiting (Golding, 1998). We reason that this predictability in an individual's sensitivity to nauseogenic stimuli could be partially attributed to their underlying neuroanatomy. Here, we specifically focused on the subcortex because of its relationship to the central autonomic network (Critchley & Harrison, 2013; Aziz & Ruffle, 2018). To that end, we identified four subcortical nuclei displaying variation in their shape (or 'morphology') dependent on *increasing* nausea, i.e. the left amygdala, right caudate and bilateral putamen.

Notably, the amygdala has a key role in the central autonomic network (Benarroch, 1993), and the involvement of basal ganglia regions in a sympathetic-related stress response is in keeping with previous findings from separate studies/datasets (Borsook *et al.* 2010; Ruffle *et al.* 2018*b*).

Nausea-related subcortical morphology may be sympathetically related. The association of these particular subcortical nuclei to nausea severity is intriguing, given that in a separate group of individuals
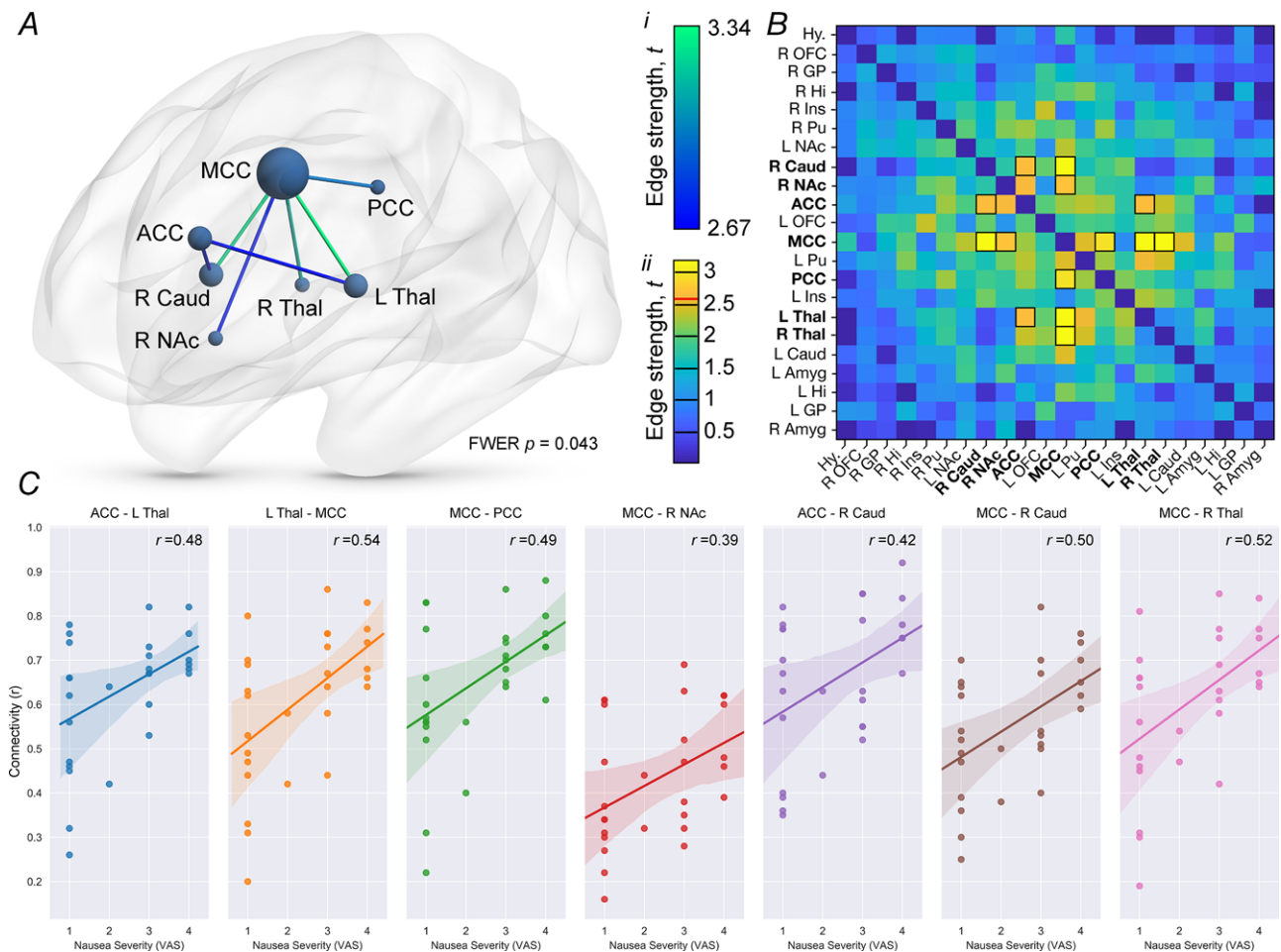

Figure 3. A novel functional brain network related to nausea severity
A, network-based statistics identified a significant functional brain network implicating 7 nodes of our *a priori* defined 22, all of which had edge strengths >2.64, equivalent to a medium effect size Cohen's *d* of >0.5. Nodes are sized according to their degree centrality (number of significant functional connections, or 'edges'). Edges are colour coded according to strength of effect size (see colour key *i*). *B*, edge-strength colour map of all nodes tested with network-based statistics, wherein edges are colour coded according to strength of effect size (see colour key *ii*, wherein a red line demarcates the critical edge strength for inclusion in the functional network). Functional connections included in the network have been outlined in black. *C*, pairwise connectivity values (i.e. between a given 2 nodes) of the functional network, scatter-plotted against nausea severity (VAS). *n* = 28. Line of best fit from linear regression with python robust outlier fitting, shaded area represents 95% confidence interval. Abbreviations: ACC, anterior cingulate cortex; Amyg, amygdala; Caud, caudate nucleus; FWER, family wise error rate; GP, globus pallidus; Hi, hippocampus; Hy, hypothalamus; Ins, insula cortex; L, left; MCC, mid-cingulate cortex; NAc, nucleus accumbens; OFC, orbitofrontal cortex; PCC, posterior cingulate cortex; Pu, putamen; R, right; Thal, thalamus; VAS, visual analogue score. [Colour figure can be viewed at wileyonlinelibrary.com]

we have previously shown that these nuclei vary in shape or volume depending on either resting sympathetic or parasympathetic tone (see Ruffle *et al.* 2018*b*). Additionally, the notion that the basal ganglia and amygdala have a regulatory function in ANS physiology has been previously described (Pazo *et al.* 1981; Nalivaiko & Blessing, 2001; Blessing, 2003). It is somewhat expected therefore that in repeating this analysis with controlled-regression of each participant's sympathetic tone, which we posit is pro-nauseogenic as described in previous studies (Farmer *et al.* 2015; Kenward *et al.* 2015; Singh *et al.* 2016; Kvale *et al.* 1991), these anatomical areas became almost entirely non-significant.

A novel functional brain network relates to severity of nausea experienced

We identified a novel network of functional connectivity, which represents the extent of information transmission and synchrony between multiple brain regions whilst exposed to a nauseous stimulus. In the processing of an inherently complex interoceptive phenomenon such as nausea, it seems highly likely that this percept is a result of multiple areas of the brain interacting at a given time. As such, this study aims to build upon previous studies of brain activity or connectivity between two brain regions only (Farmer *et al.* 2015; Toschi *et al.* 2017).
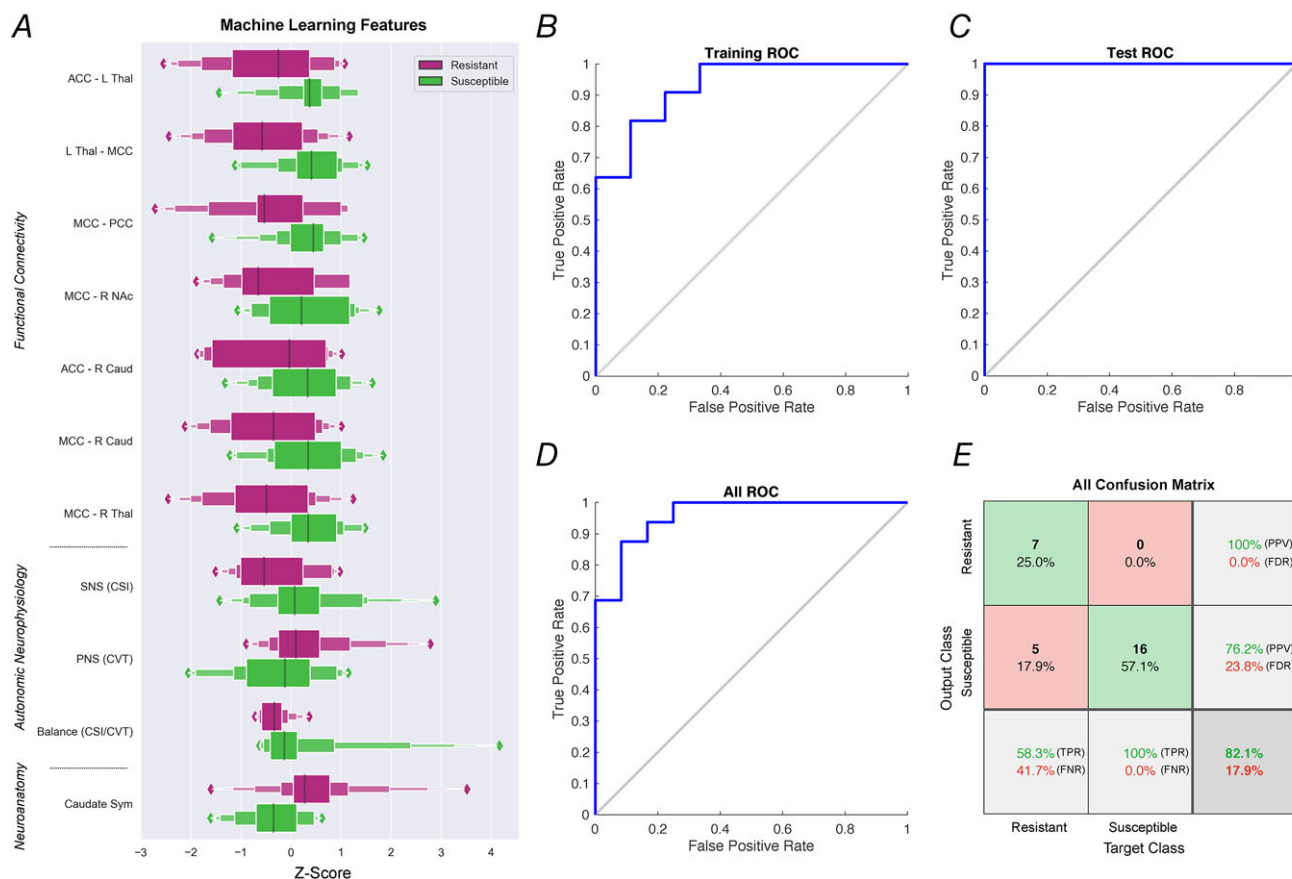

Figure 4. Proof of concept: a machine learning neural network to predict susceptibility or resistance to nausea

A, a machine learning neural network was trained to predict susceptibility to nausea in the form of a binary classifier (i.e. susceptible or resistant). Eleven feature vectors were used in this model: 7 functional connections of the identified nausea network (see Fig. 3), resting CVT, CSI, CSI/CVT ratio (see Fig. 1) and caudate volumetric symmetry ratios, derived from further feature selection. Exponential box plots illustrate the relationship of one feature to nausea resistance (purple) or susceptible (green), on a *Z*-scored *x*-axis. *B*, receiver operator characteristic (ROC) curve of training state. The model was *trained* to an initial accuracy of 80% (AUC 0.80) with random data division, utilizing 70% of total samples. *C*, ROC curve of testing state. *Test* subsample (15%) correctly identified according to nausea susceptible at 100% accuracy. *D*, total ROC for all data partitions (AUC 0.82). *E*, confusion matrix for total predictive network properties. Abbreviations: ACC, anterior cingulate cortex; AUC, area under the curve; Caud, caudate nucleus; CSI, cardiac sympathetic index; CVT, cardiac vagal tone; FDR, false discovery rate; FNR, false negative rate; L, left; MCC, mid-cingulate cortex; NAc, nucleus accumbens; PCC, posterior cingulate cortex; PPV, positive predictive value; R, right; ROC, receiver operator characteristic; Sym, symmetry; Thal, thalamus; TPR, true positive rate. [Colour figure can be viewed at wileyonlinelibrary.com]

In particular, we identified a network which increased in strength (functional connectivity/information transfer) with increasing nausea severity, which encompassed the anterior, mid- and posterior cingulate cortices, both sides of the thalamus, right caudate nucleus and nucleus accumbens. Some of these regions have known associations to nausea (Napadow *et al.* 2013*b*; Farmer *et al.* 2015; Sclocco *et al.* 2016; Toschi *et al.* 2017), although their co-relationship to autonomic neurophysiology seems salient and will be elaborated on below.

The identified brain network of nausea severity was related to autonomic neurophysiology. Notably, the connectivity of the identified nausea-severity network correlated positively with both resting sympathetic nervous system tone and sympathovagal balance. As already stipulated above, given a presupposition of increased/elevated sympathetic tone as pro-nauseogenic (Farmer *et al.* 2015; reviewed in Kenward *et al.* 2015; Singh *et al.* 2016), it is interesting to also find a concomitant autonomic association to this network, wherein greater connectivity corresponded both to greater nausea severity and resting sympathetic tone. We have already discussed some of these brain regions and their known role in autonomic regulation, though in this network we additionally implicate the thalamus, cingulate cortex and nucleus accumbens, all of which are known to have a role in sympathetic neuro-regulation, or a sympathetic response to events meriting emotional arousal (such as nausea or pain) (Critchley & Harrison, 2013; Ruffle *et al.* 2018*a,b*). Hence, it is reasonable to suggest that this neural network reflects SNS-related nausea processing. Future work should investigate if a trilinear relationship between this functional brain network, autonomic measures and GI measures (such as with electrogastrogram or self-reported epigastric symptoms) exist in real-time synchrony. It would be prudent to also investigate additional nauseogenic stimuli in this context, including non-visual, to ensure no confound from visual processing/saccades (though our data here was compared to a control visual stimulus). Furthermore, investigation with measures of attention, and arousal and stress would be useful for future study to examine their relationship to these findings.

Artificial intelligence to predict nausea susceptibility

Lastly, as a proof of concept, we illustrate how complex neurophysiological data, such as functional connectivity, neuroanatomy and autonomic neurophysiology can be coalesced with machine learning to build a model to predict sensitivity or resistance to nausea, induced by VIMS. In the last few years, interest in machine learning has increased exponentially, and its application to academia and healthcare is rapidly developing (Ruffle *et al.* 2018*d*). However, the use of this technology in predicting difficult or 'softer' endpoints, such as subjective reporting of nausea, presents an intriguing clinical opportunity. It should be noted, however, that this model aimed to reflect a proof of concept *only* and limitations do exist, namely that a larger sample size and disparate nausea-inducing stimuli would be required to further develop such a network for either future academic work or for deployment in a healthcare setting. That being said, this proof of concept model alone led to a high level of accuracy, raising the question of whether machine learning with such brain data could be used to predict susceptibility to unpleasant experiences, such as nausea and visceral pain.

Conclusions

In this study, we build on previous studies investigating brain activity related to nausea and illustrate the brain processing of nausea as a functional network. To our knowledge, this is the first study using network analysis to describe how multiple brain regions communicate to give rise to the perception of nausea. The study is also the first to investigate the interrelationship between subcortical morphology and predisposition to nausea, not least by demonstrating its close-knit relationship to autonomic neurophysiology (Ruffle *et al.* 2018*b*). Finally, as a proof of concept, we illustrated how a given individual's underlying neuroanatomy, functional connectivity and autonomic neurophysiology can be coalesced to predict susceptibility or resistance to nausea, using a novel machine learning approach. Future work should interrogate the use of machine learning to predict nausea susceptibility (including from multiple nauseogenic stimuli), be it from brain data, autonomic or otherwise to determine if the described brain functional connectivity parameters could act as biomarkers to study the efficacy of novel nausea therapies.

References

Anderson MJ & Robinson J (2008). Permutation tests for linear models. *Aust N Z J Stat* **43**, 75–88.

Andrews PL & Sanger GJ (2014). Nausea and the quest for the perfect anti-emetic. *Eur J Pharmacol* **722**, 108–121.

Angeli TR, Cheng LK, Du P, Wang TH, Bernard CE, Vannucchi MG, Faussone-Pellegrini MS, Lahr C, Vather R, Windsor JA, Farrugia G, Abell TL & O'Grady G (2015). Loss of interstitial cells of cajal and patterns of gastric dysrhythmia in patients with chronic unexplained nausea and vomiting. *Gastroenterology* **149**, 56–66.e55.

Aziz Q & Ruffle JK (2018). The neurobiology of gut feelings. In *The Interoceptive Basis of the Mind*, eds Tsakiris M & De Preester H, pp. 1–46. Oxford University Press.

Baroncini M, Jissendi P, Balland E, Besson P, Pruvo JP, Francke JP, Dewailly D, Blond S & Prevot V (2012). MRI atlas of the human hypothalamus. *Neuroimage* **59**, 168–180.

Benarroch EE (1993). The central autonomic network: functional organization, dysfunction, and perspective. *Mayo Clin Proc* **68**, 988–1001.

Blessing WW (2003). Lower brainstem pathways regulating sympathetically mediated changes in cutaneous blood flow. *Cell Mol Neurobiol* **23**, 527–538.

Borsook D, Upadhyay J, Chudler EH & Becerra L (2010). A key role of the basal ganglia in pain and analgesia – insights gained through human functional imaging. *Mol Pain* **6**, 27.

Brock C, Jessen N, Brock B, Jakobsen PE, Hansen TK, Rantanen JM, Riahi S, Dimitrova YK, Dons-Jensen A, Aziz Q, Drewes AM & Farmer AD (2017). Cardiac vagal tone, a non-invasive measure of parasympathetic tone, is a clinically relevant tool in Type 1 diabetes mellitus. *Diabet Med* **34**, 1428–1434.

Bubka A & Bonato F (2003). Optokinetic drum tilt hastens the onset of vection-induced motion sickness. *Aviat Space Environ Med* **74**, 315–319.

Critchley HD & Harrison NA (2013). Visceral influences on brain and behavior. *Neuron* **77**, 624–638.

Dey A (2016). Machine learning algorithms: A review. *IJCSIT* **7**, 1174–1179.

European Society of Cardiology (1996). Heart rate variability: standards of measurement, physiological interpretation and clinical use. Task Force of the European Society of Cardiology and the North American Society of Pacing and Electrophysiology. *Circulation* **93**, 1043–1065.

Farmer AD, Ban VF, Coen SJ, Sanger GJ, Barker GJ, Gresty MA, Giampietro VP, Williams SC, Webb DL, Hellstrom PM, Andrews PL & Aziz Q (2015). Visually induced nausea causes characteristic changes in cerebral, autonomic and endocrine function in humans. *J Physiol* **593**, 1183–1196.

Farmer AD, Coen SJ, Kano M, Weltens N, Ly HG, Botha C, Paine PA, Oudenhove LV & Aziz Q (2014). Normal values and reproducibility of the real-time index of vagal tone in healthy humans: a multi-center study. *Ann Gastroenterol* **27**, 362–368.

Farmer AD, Coen SJ, Kano M, Worthen SF, Rossiter HE, Navqi H, Scott SM, Furlong PL & Aziz Q (2013). Psychological traits influence autonomic nervous system recovery following esophageal intubation in health and functional chest pain. *Neurogastroenterol Motil* **25**, 950-e772.

Freedman D & Lane D (1983). A nonstochastic interpretation of reported significance levels. *J Bus Econ Stat* **1**, 292–298.

Gianaros PJ, Muth ER, Mordkoff JT, Levine ME & Stern RM (2001). A questionnaire for the assessment of the multiple dimensions of motion sickness. *Aviat Space Environ Med* **72**, 115–119.

Golding JF (1998). Motion sickness susceptibility questionnaire revised and its relationship to other forms of sickness. *Brain Res Bull* **47**, 507–516.

Golding JF, Doolan K, Acharya A, Tribak M & Gresty MA (2012). Cognitive cues and visually induced motion sickness. *Aviat Space Environ Med* **83**, 477–482.

Haug TT, Mykletun A & Dahl AA (2002). The prevalence of nausea in the community: psychological, social and somatic factors. *Gen Hosp Psychiatry* **24**, 81–86.

Julu PO (1992). A linear scale for measuring vagal tone in man. *J Auton Pharmacol* **12**, 109–115.

Julu PO & Hondo RG (1992). Effects of atropine on autonomic indices based on electrocardiographic R-R intervals in healthy volunteers. *J Neurol Neurosurg Psychiatry* **55**, 31–35.

Kennedy RS, Drexler J & Kennedy RC (2010). Research in visually induced motion sickness. *Appl Ergon* **41**, 494–503.

Kenward H, Pelligand L, Savary-Bataille K & Elliott J (2015). Nausea: current knowledge of mechanisms, measurement and clinical impact. *Vet J* **203**, 36–43.

Koch KL (1999). Illusory self-motion and motion sickness: a model for brain-gut interactions and nausea. *Dig Dis Sci* **44**, 53S–57S.

Kvale G, Hugdahl K, Asbjørnsen A, Rosengren B, Lote K & Nordby H (1991). Anticipatory nausea and vomiting in cancer patients. *J Consult Clin Psychol* **59**, 894–898.

Little CJ, Julu PO, Hansen S & Reid SW (1999). Real-time measurement of cardiac vagal tone in conscious dogs. *Am J Physiol Heart Circ Physiol* **276**, H758–H765.

Miller EF 2nd & Graybiel A (1970). A provocative test for grading susceptibility to motion sickness yielding a single numerical score. *Acta Otolaryngol Suppl* **274**, 1–20.

Muth ER (2006). Motion and space sickness: intestinal and autonomic correlates. *Auton Neurosci* **129**, 58–66.

Nalivaiko E & Blessing WW (2001). Raphe region mediates changes in cutaneous vascular tone elicited by stimulation of amygdala and hypothalamus in rabbits. *Brain Res* **891**, 130–137.

Napadow V, Sheehan J, Kim J, Dassatti A, Thurler AH, Surjanhata B, Vangel M, Makris N, Schaechter JD & Kuo B (2013*a*). Brain white matter microstructure is associated with susceptibility to motion-induced nausea. *Neurogastroenterol Motil* **25**, 448–450, e303.

Napadow V, Sheehan JD, Kim J, Lacount LT, Park K, Kaptchuk TJ, Rosen BR & Kuo B (2013*b*). The brain circuitry underlying the temporal evolution of nausea in humans. *Cereb Cortex* **23**, 806–813.

Oldfield RC (1971). The assessment and analysis of handedness: the Edinburgh inventory. *Neuropsychologia* **9**, 97–113.

Patenaude B, Smith SM, Kennedy DN & Jenkinson M (2011). A Bayesian model of shape and appearance for subcortical brain segmentation. *Neuroimage* **56**, 907–922.

Pazo JH, Tumilasci OR & Medina JH (1981). Studies on the mechanisms of L-dopa-induced salivary secretion. *Eur J Pharmacol* **69**, 255–261.

Ruffle JK, Aziz Q & Farmer AD (2018*a*). Pro-nociceptive effects mediated by adenosinergic A2A activity at the nucleus accumbens; but what about the autonomic nervous system? *Pain* **159**, 997.

Ruffle JK, Coen SJ, Giampietro V, Williams SCR, Apkarian AV, Farmer AD & Aziz Q (2018*b*). Morphology of subcortical brain nuclei is associated with autonomic function in healthy humans. *Hum Brain Mapp* **39**, 381–392.

Ruffle JK, Coen SJ, Giampietro V, Williams SCR, Aziz Q & Farmer AD (2018*c*). Preliminary report: parasympathetic tone links to functional brain networks during the anticipation and experience of visceral pain. *Sci Rep* **8**, 13410.

Ruffle JK, Farmer AD & Aziz Q (2018*d*). Artificial intelligence assisted gastroenterology - promises and pitfalls. *Am J Gastroenterol* (in press; https://doi.org/10.1038/s41395-018-0268-4).

Ruffle JK, Frokjaer JB & Farmer AD (2017). Neuroimaging of visceral pain. In *Neuroimaging of Pain*, ed. Saba L, pp. 341–374. Springer International Publishing.

Russell SJ & Norvig P (2009). *Artificial Inteliigence, A Modern Approach.* Pearson Education.

Sanger GJ & Andrews PLR (2018). A history of drug discovery for treatment of nausea and vomiting and the implications for future research. *Front Pharmacol* **9**, 913.

Sclocco R, Kim J, Garcia RG, Sheehan JD, Beissner F, Bianchi AM, Cerutti S, Kuo B, Barbieri R & Napadow V (2016). Brain circuitry supporting multi-organ autonomic outflow in response to nausea. *Cereb Cortex* **26**, 485–497.

Shupak A & Gordon CR (2006). Motion sickness: advances in pathogenesis, prediction, prevention, and treatment. *Aviat Space Environ Med* **77**, 1213–1223.

Singh P, Yoon SS & Kuo B (2016). Nausea: a review of pathophysiology and therapeutics. *Therap Adv Gastroenterol* **9**, 98–112.

Smith SM, Jenkinson M, Woolrich MW, Beckmann CF, Behrens TE, Johansen-Berg H, Bannister PR, De Luca M, Drobnjak I, Flitney DE, Niazy RK, Saunders J, Vickers J, Zhang Y, De Stefano N, Brady JM & Matthews PM (2004). Advances in functional and structural MR image analysis and implementation as FSL. *Neuroimage* **23** (Suppl. 1), S208–219.

Sporns O, Tononi G & Kötter R (2005). The human connectome: A structural description of the human brain. *PLoS Comput Biol* **1**, e42.

Stern RM, Koch KL & Andrews P (2011). *Nausea: mechanisms and management.* Oxford University Press, New York.

Talairach J & Tournoux P (1988). *Co-Planar Stereotaxic Atlas of the Human Brain: 3-D Proportional System: An Approach to Cerebral Imaging: 3-Dimensional Proportional System: An Approach to Cerebral Imaging.* Thieme Publishers.

Toichi M, Sugiura T, Murai T & Sengoku A (1997). A new method of assessing cardiac autonomic function and its comparison with spectral analysis and coefficient of variation of R-R interval. *J Auton Nerv Syst* **62**, 79–84.

Toschi N, Kim J, Sclocco R, Duggento A, Barbieri R, Kuo B & Napadow V (2017). Motion sickness increases functional connectivity between visual motion and nausea-associated brain regions. *Auton Neurosci* **202**, 108–113.

Xia M, Wang J & He Y (2013). BrainNet Viewer: a network visualization tool for human brain connectomics. *PLoS One* **8**, e68910.

Yarkoni T, Poldrack RA, Nichols TE, Van Essen DC & Wager TD (2011). NeuroSynth: a new platform for large-scale automated synthesis of human functional neuroimaging data. Front Neuroinform Conference Abstract: 4th INCF Congress of Neuroinformatics. https://doi.org/10.3389/conf.fninf.2011.08.00058.

Zalesky A, Fornito A & Bullmore ET (2010). Network-based statistic: identifying differences in brain networks. *Neuroimage* **53**, 1197–1207.

Zigmond AS & Snaith RP (1983). The hospital anxiety and depression scale. *Acta Psychiatr Scand* **67**, 361–370.

Additional information

Competing interests

None of the authors have any conflict of interests to declare.

Author contributions

J.R., A.P., A.D.F.: acquisition of data; manuscript preparation; statistical analysis; study supervision; critical revision of the manuscript for important intellectual content. V.G., M.A.H.: acquisition of data; critical revision of the manuscript for important intellectual content. G.S., P.A., S.C.R.W., Q.A.: pioneered study concept and design, technical or material support; obtained funding as principal applicant; critical revision of the manuscript for important intellectual content, project supervision. All authors have approved the final version of the manuscript and agree to be accountable for all aspects of the work. All persons designated as authors qualify for authorship, and all those who qualify for authorship are listed.

Funding

Acknowledgements

Supporting information

Additional supporting information may be found online in the Supporting Information section at the end of the article.

Figure S1. MSSQ score alone is a *poor* predictor of nausea.
Figure S2. Relationship of functional connectivity to sympathetic tone.
Figure S3. Relationship of functional connectivity to parasympathetic tone.
Figure S4. Relationship of functional connectivity to sympathovagal balance.
Video S1. 3D movie of a novel functional brain network of nausea severity.